Journal of Nanobiotechnology

RESEARCH

Open Access

Hepatocyte-derived tissue extracellular vesicles safeguard liver regeneration and support regenerative therapy

Si-Qi Ying[1†], Yuan Cao[1,2†], Ze-Kai Zhou[1,3], Xin-Yan Luo[1,3], Xiao-Hui Zhang[1,2], Ke Shi[1,4], Ji-Yu Qiu[5], Shu-Juan Xing[1,6], Yuan-Yuan Li[1], Kai Zhang[1,7], Fang Jin[1,2], Chen-Xi Zheng[1*], Yan Jin[1,4*] and Bing-Dong Sui[1*]

Abstract

Tissue-derived extracellular vesicles (EVs) are emerging as pivotal players to maintain organ homeostasis, which show promise as a next-generation candidate for medical use with extensive source. However, the detailed function and therapeutic potential of tissue EVs remain insufficiently studied. Here, through bulk and single-cell RNA sequencing analyses combined with ultrastructural tissue examinations, we first reveal that in situ liver tissue EVs (LT-EVs) contribute to the intricate liver regenerative process after partial hepatectomy (PHx), and that hepatocytes are the primary source of tissue EVs in the regenerating liver. Nanoscale and proteomic profiling further identify that the hepatocyte-specific tissue EVs (Hep-EVs) are strengthened to release with carrying proliferative messages after PHx. Moreover, targeted inhibition of Hep-EV release *via* AAV-sh*Rab27a in vivo* confirms that Hep-EVs are required to orchestrate liver regeneration. Mechanistically, Hep-EVs from the regenerating liver reciprocally stimulate hepatocyte proliferation by promoting cell cycle progression through Cyclin-dependent kinase 1 (Cdk1) activity. Notably, supplementing with Hep-EVs from the regenerating liver demonstrates translational potential and ameliorates insufficient liver regeneration. This study provides a functional and mechanistic framework showing that the release of regenerative Hep-EVs governs rapid liver regeneration, thereby enriching our understanding of physiological and endogenous tissue EVs in organ regeneration and therapy.

Keywords Liver regeneration, Partial hepatectomy, Hepatocytes, Extracellular vesicles, Cell cycle

[†]Si-Qi Ying and Yuan Cao contributed equally to this work.

*Correspondence:
Chen-Xi Zheng
chenxizheng@fmmu.edu.cn
Yan Jin
yanjin@fmmu.edu.cn
Bing-Dong Sui
bingdong@fmmu.edu.cn

[1]State Key Laboratory of Oral & Maxillofacial Reconstruction and Regeneration, National Clinical Research Center for Oral Diseases, Shaanxi International Joint Research Center for Oral Disease, Center for Tissue Engineering, School of Stomatology, The Fourth Military Medical University, Xi'an, Shaanxi 710032, China
[2]Department of Orthodontics, School of Stomatology, The Fourth Military Medical University, Xi'an, Shaanxi 710032, China
[3]School of Basic Medicine, The Fourth Military Medical University, Xi'an, Shaanxi 710032, China
[4]Xi'an Institute of Tissue Engineering and Regenerative Medicine, Xi'an, Shaanxi 710032, China
[5]Department of VIP Dental Care, School of Stomatology, The Fourth Military Medical University, Xi'an, Shaanxi 710032, China
[6]College of Life Science, Northwest University, Xi'an, Shaanxi 710069, China
[7]Department of Oral and Maxillofacial Surgery, School of Stomatology, The Fourth Military Medical University, Xi'an, Shaanxi 710032, China

Introduction

The liver, the largest solid organ in the body, critically maintains metabolism and serves as the central hub for detoxification. To cope with daily challenges, the liver has developed a potent, robust, and finely tuned regenerative capability, capable of fully regenerating up to two-thirds of its total parenchyma [1, 2]. Liver regeneration involves a complex cellular interplay, primarily centered around hepatocytes but also encompassing biliary cells and various non-parenchymal cells (NPCs) [3]. In a healthy liver, hepatocytes are typically mitotically quiescent; however, following toxic damage or surgical resection, they can rapidly enter the cell cycle and proliferate. This proliferation is coordinated with the immune, endothelial, and stromal components, working synergistically to restore liver mass and function [4–8]. This hepatocyte expansion-related cellular coordination is recognized as being mediated by diverse paracrine cytokines, which are essential for ensuring efficient liver regeneration and are a prerequisite for proper organismal functioning [4, 5, 9]. However, the regenerative capacity of the liver can be overwhelmed or suppressed under conditions of extensive injury or progressive damage, resulting in hepatic diseases that pose a global medical challenge [10, 11]. Further exploration of the mechanisms underlying liver regeneration is crucial for developing viable strategies for hepatic disease therapy.

Extracellular vesicles (EVs) are emerging as a novel form of intercellular communication that regulates a variety of biological processes, characterized by their functionalized surface molecules and encapsulated cargoes, including proteins, nucleic acids, and lipids [12, 13]. Solid tissues and organs are increasingly recognized as natural reservoirs of endogenous EVs, with tissue-derived EVs playing a significant role in reflecting and regulating tissue health and disease statuses [14, 15]. A recent study has isolated tissue EVs from the kidney and skin, which have been applied to promote target tissue repair in a donor tissue-specific manner following allogeneic transplantation [16]. It has also been reported that liver tissue EVs (denoted LT-EVs), isolated from both normal and carbon tetrachloride (CCl_4)-induced damaged livers, accelerate the recovery of liver tissues from CCl_4-induced hepatic necrosis after administration [17]. However, due to the heterogeneous nature of tissue-resident cells and the imprecise properties of the bulk isolation method for tissue EVs, there remains an unmet need to characterize the detailed endogenous EV populations contributing to tissue physiology and pathology [18–20]. In terms of liver regeneration, EVs derived from the cultured hepatocyte supernatant have demonstrated efficacy in promoting liver regeneration post-infusion [21]. We have also recently reported that circulatory apoptotic EVs contribute to liver regeneration [22]. However, whether LT-EVs from hepatocytes or any other cell types specifically participate in the liver regeneration process has not been rigorously evaluated in situ.

Here, we aimed to investigate the role and mechanisms of tissue-derived, cell-specific functional EV populations that potentially safeguard liver regeneration. By conducting unbiased examinations of the liver transcriptome *via* bulk RNA sequencing (RNA-seq) and the hepatic cell landscape *via* single-cell RNA sequencing (scRNA-seq), we demonstrated that hepatocytes are the primary source of intercellular communication in the regenerating liver after partial hepatectomy (PHx). These cells are programmed to enrich biogenesis and release of EVs. Furthermore, we first performed ultrastructural observations of LT-EVs in situ and established an immunomagnetic sorting protocol to analyze hepatocyte-specific LT-EVs marked by the featured asialoglycoprotein receptor (ASGPR) (denoted Hep-EVs). These Hep-EVs reveal enhanced release at the nanoscale with proliferative information identified at the high-throughput proteomic level during liver regeneration. Subsequently, through targeted inhibition of hepatocyte EV release *in vivo via* adeno-associated virus (AAV)-mediated short heparin RNA (shRNA) knockdown of GTPase *Rab27a* expression, we discovered that Hep-EVs are indispensable for orchestrating liver regeneration. Mechanistically, Hep-EVs from the regenerating liver were shown to reciprocally stimulate the proliferation of hepatocytes through promoting cell cycle progression, which function *via* and are hallmarked by Cyclin-dependent kinase 1 (Cdk1) activity. Importantly, replenishment of Hep-EVs from regenerating livers holds translational promise and rescues insufficient liver regeneration. Therefore, our study establishes a functional and mechanistic framework in which the release of regenerative Hep-EVs governs rapid liver regeneration, shedding light on the investigation of physiological and endogenous tissue EV populations in organ regeneration and therapy.

Results

Active involvement of in situ LT-EVs in the regeneration process after PHx

Initially, we employed the PHx model, which facilitates the study of liver regeneration without significant necrosis [1, 2]. As anticipated, hepatocyte proliferation was confirmed at 72 h after 2/3 PHx by immunofluorescence (IF) staining, accompanied by increased macrophage inflammation and activation of liver sinusoidal endothelial cells (LSECs) and hepatic stellate cells (HSCs), indicating regenerative responses at the organ level (Figure S1A and B). Subsequent analysis through liver bulk RNA sequencing was conducted to explore potential events during the regenerative process. Among the 9,388 overlapping genes detected between Sham and PHx livers

(Fig. 1A), 1,009 were identified as differentially expressed genes (DEGs) (Fig. 1B and Table S1), showing characteristics enriched in cell cycle regulation and cell division, as evidenced by the Gene Ontology (GO) analysis (Fig. 1C). Notably, there was a significant enrichment of DEGs in multiple EV-related terms, such as "extracellular exosome", "extracellular vesicle", and "regulation of vesicle-mediated transport" (Fig. 1D). Kyoto Encyclopedia of Genes and Genomes (KEGG) analysis and Gene Set Enrichment Analysis (GSEA) confirmed the property of cell cycle control of DEGs, which was upregulated in the PHx group (Fig. 1E and F). Particularly, for the terms "extracellular exosome" and "extracellular vesicle", GSEA demonstrated significant upregulation in the PHx liver compared to the Sham control, underscoring the involvement of EVs in liver regeneration (Fig. 1F). To identify potential EVs in the liver tissues, we conducted transmission electron microscopy (TEM) analysis. Intriguingly, vesicle-like nanoparticles were observed in the extracellular space adjacent to hepatocytes, present in the Sham liver but showing an increase in abundance in the PHx liver (Fig. 1G). Nanosized vesicles were also detected in interstitial spaces between hepatocytes and macrophages or endothelial cells (ECs) in both Sham and PHx livers (Figure S1C). These findings collectively suggest the active involvement of in situ EVs in liver regeneration.

Hepatocytes are the major origin of LT-EVs during liver regeneration

Next, we examined the origin of LT-EVs in the liver regeneration process. Accordingly, we re-analyzed two scRNA-seq datasets from mouse liver under Sham and PHx conditions (GSM4572241 and GSM4572244). Cell clustering visualized through t-distributed stochastic neighbor embedding (tSNE) plots identified eight distinct liver cell types, with a decrease in the proportion of hepatocytes after PHx (Fig. 2A and B). Despite this decreased proportion, pseudotime analysis indicated that hepatocytes from Sham and PHx livers occupied distinct stage branches, with some cells transitioning, suggesting a shift in cellular state (Figure S2A). A total of 3,524 DEGs between Sham and PHx hepatocytes were identified (Fig. 2C), categorized based on functional annotations from GO and KEGG databases, such as the GO term "cellular anatomical entity" and the KEGG term "transport and catabolism" (Figure S2B and C). Further in-depth analysis of the functional implications of these DEGs demonstrated remarkable enrichment of EV-related GO terms, particularly associated with EV assembly and secretion (Fig. 2D). These results suggest that hepatocytes might be programmed for biogenesis and release of EVs in liver regeneration.

We then performed flow cytometric analysis on collected LT-EVs to investigate the surface antigens inherited from their parental cells. Interestingly, ASGPR-marked LT-EVs, primarily derived from hepatocytes (i.e., Hep-EVs), constituted the largest portion of total LT-EVs in the physiological state (mean percentage approximately 31%) and demonstrated an approximate two-fold increase after PHx (Fig. 2E). Other significant components of Sham LT-EVs, which decreased after PHx, included those from biliary epithelial cells (marked by cytokeratin 19, CK19) and B cells (marked by CD19) (Fig. 2E). LT-EV subpopulations with increased proportions during liver regeneration included those from F4/80-marked Kupffer cells and CD31-marked ECs. In contrast, LT-EVs from liver-infiltrated monocyte-derived macrophages (MoMFs, marked by CD11b), hepatic stellate cells (HSCs, marked by glial fibrillary acidic protein, GFAP), and T cells (marked by CD3) constituted only around or below 5% of the total (Fig. 2E). Correspondingly, we identified previously unrecognized cell origins of LT-EVs (Fig. 2F). Collectively, these results suggest that hepatocytes are the principal source of LT-EVs and serve as the key mediators of intercellular EV communication during liver regeneration.

Hep-EVs reveal enhanced release with proliferative information in liver regeneration

To specifically analyze Hep-EVs during liver regeneration, we next established a comprehensive protocol for collecting and characterizing antigen-specific tissue EVs by immunomagnetic sorting, adopting the ASGPR surface marker for Hep-EVs (Figure S3A). As anticipated, flow cytometric analysis confirmed that the $ASGPR^+$ percentage of LT-EVs was 33.79% prior to immunomagnetic sorting, and the percentage decreased to 0.10% in $ASGPR^-$ LT-EVs and increased to 98.34% in sorted Hep-EVs (Fig. 3A and Figure S3B). Following validation of this sorting efficacy, we applied this approach to investigate LT-EVs and Hep-EVs derived from both Sham and PHx mice, with EV quality evaluated according to the Minimal Information for Studies of Extracellular Vesicles 2023 (MISEV2023) [23]. Nanoparticle tracking analysis (NTA) showed that the diameters of LT-EVs from both Sham and PHx mice ranged from 50 to 500 nm, peaking at 150–200 nm (Fig. 3B). Notably, PHx mice produced a significantly greater quantity of LT-EVs compared to Sham mice, as quantified by particle number by NTA and protein content by the bicinchoninic acid (BCA) assay (Fig. 3C). Further observation by TEM revealed that LT-EVs displayed the typical cup-shaped morphology with membranous structures in both Sham and PHx conditions (Fig. 3D). Furthermore, after immunomagnetic sorting, Hep-EVs from both Sham and PHx mice maintained characteristic particle distributions in NTA (Fig. 3E), and Hep-EVs derived from PHx livers exhibited a higher yield than their Sham counterparts (Fig. 3F).

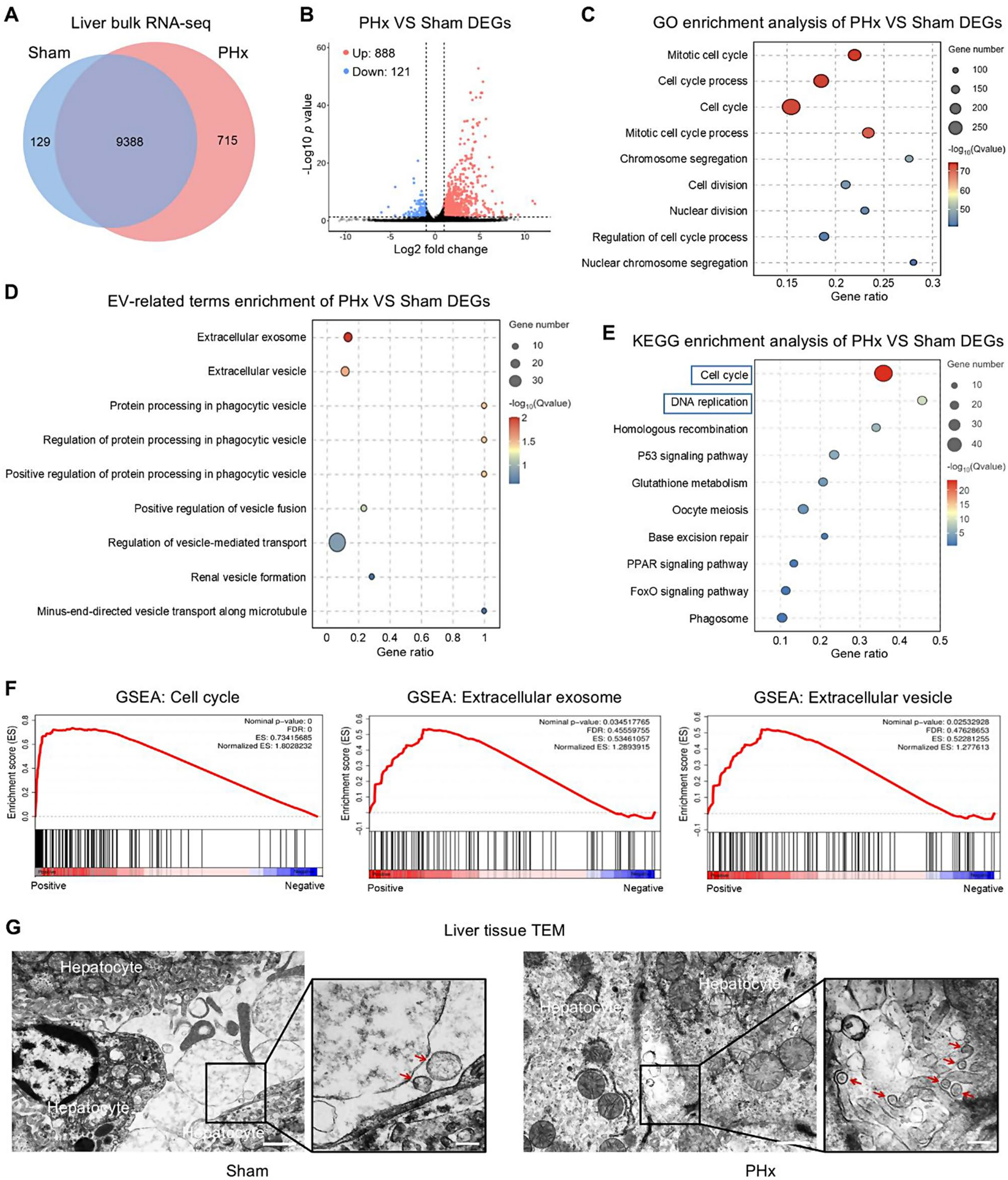

Fig. 1 LT-EVs are involved in the liver regenerative process after PHx. (**A**) Venn diagram of transcriptome of PHx and Sham livers. (**B**) Volcano plot of transcriptome of PHx and Sham livers. (**C**) GO enrichment analysis of DEGs in PHx over Sham livers. (**D**) GO terms of DEGs related to EVs enriched in PHx over Sham livers. (**E**) KEGG enrichment analysis of DEGs in PHx over Sham livers. (**F**) GSEA analysis of DEGs between PHx and Sham livers for the terms "Cell cycle", "Extracellular exosome", and "Extracellular vesicle". (**G**) TEM analysis of Sham and PHx liver tissues. Hepatocytes were identified with featured morphologies. Red arrows indicating LT-EVs in the extracellular interstitial space. Bars: 1 μm (low magnification) and 200 nm (high magnification)

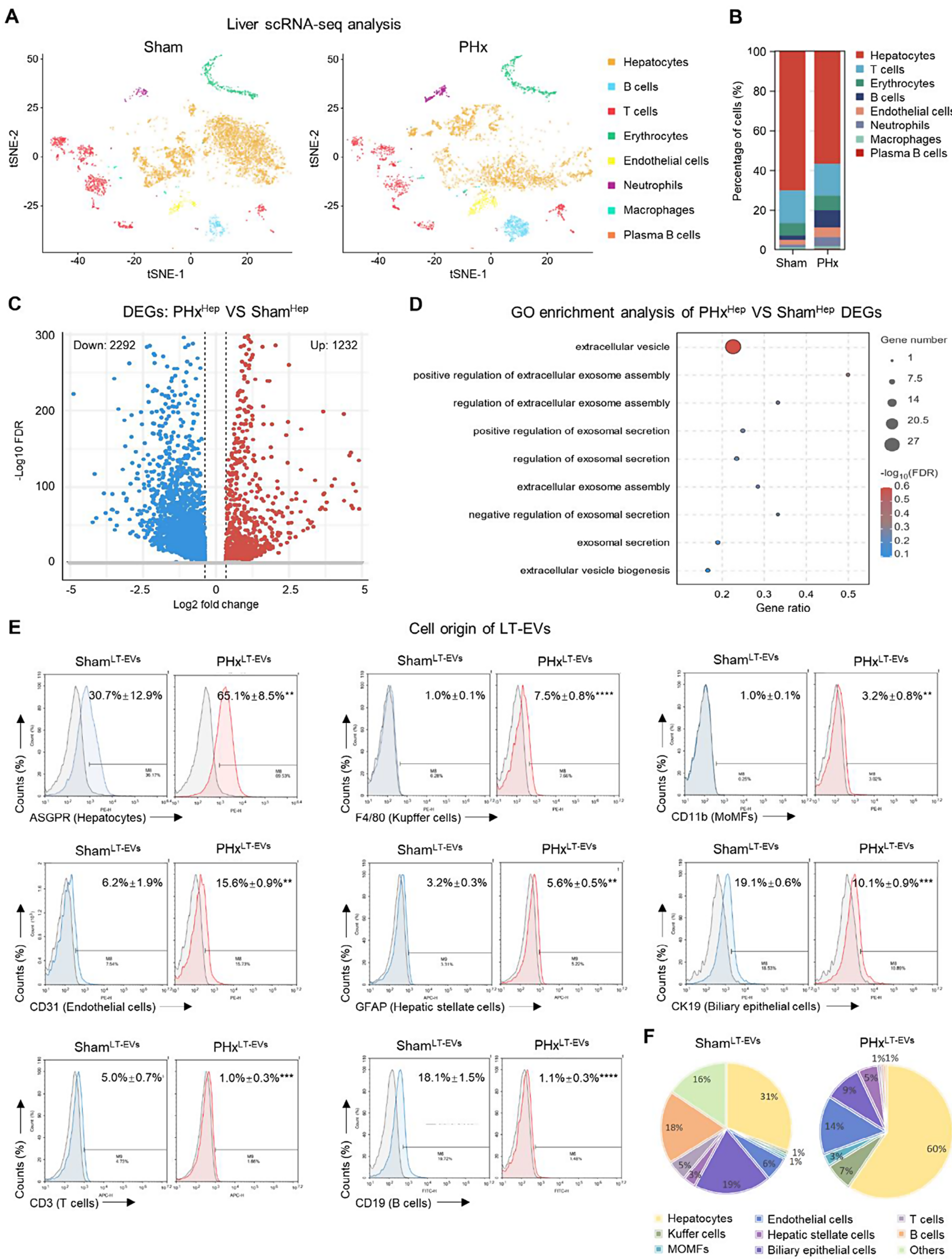

Fig. 2 Hepatocytes are the major origin of LT-EVs during liver regeneration. (**A**) tSNE plots displaying the distribution of different cell types in Sham and PHx livers. Source data were derived from the GSM4572241 and GSM4572243 series in the GEO database. (**B**) Cell type proportion in Sham and PHx livers. (**C**) Volcano plot showing DEGs between PHx and Sham hepatocytes. (**D**) GO enrichment analysis of DEGs in PHx over Sham hepatocytes. (**E**) Flow cytometric analysis of Sham and PHx LT-EVs with surface exposure of ASGPR, F4/80, CD11b, CD31, GFAP, CK19, CD3, and CD19. Corresponding isotype control groups were used to distinguish positively stained EVs. Mean ± SD. $n = 3$ per group. **, $p < 0.01$; ***, $p < 0.001$; ****, $p < 0.0001$; two-tailed Student's unpaired t tests. (**F**) Pie charts illustrating the quantification of LT-EV constitution originated from different cell types using mean values of (**E**) normalized to percentages

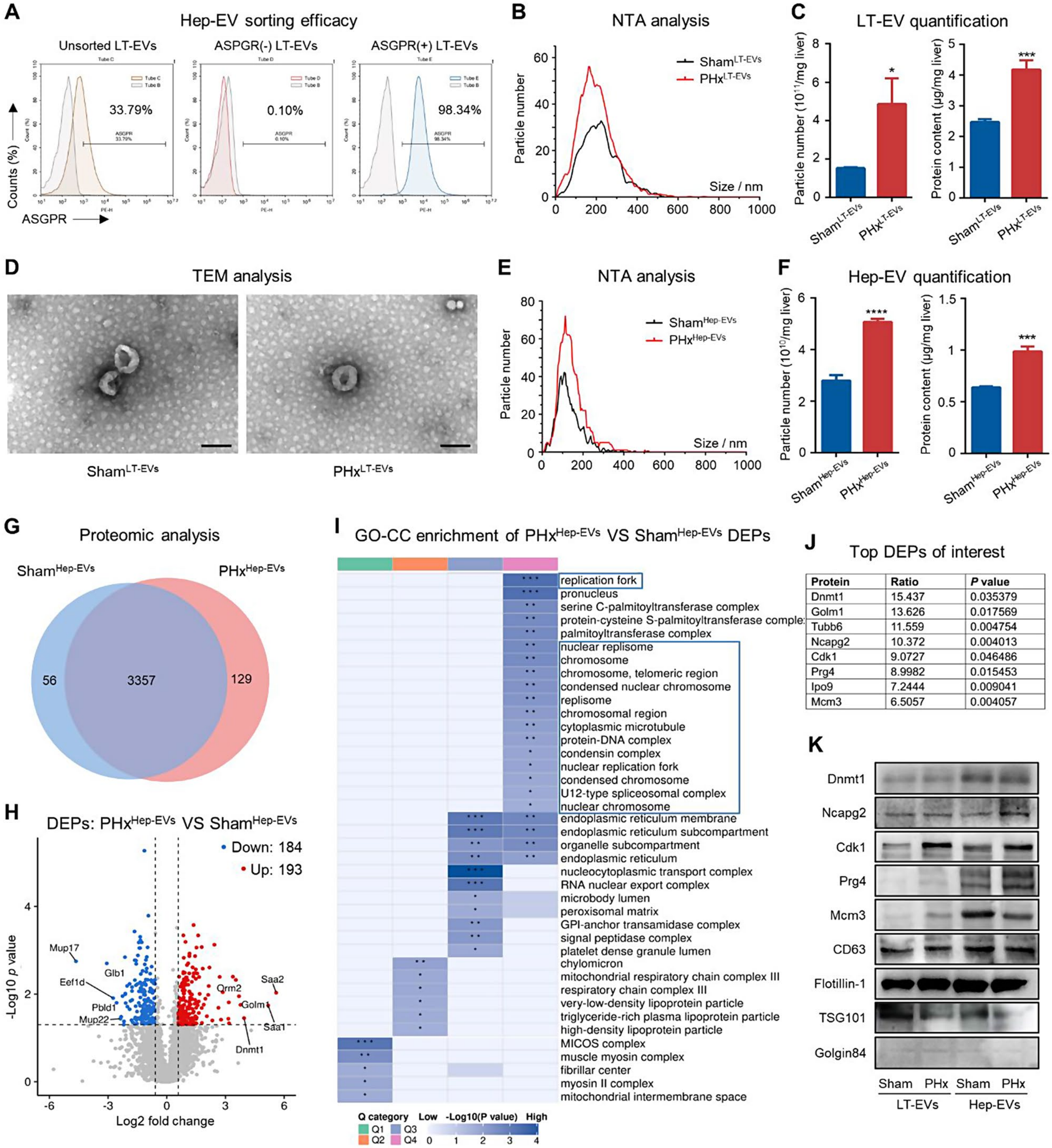

Fig. 3 Hep-EVs reveals enhanced release with proliferative information during liver regeneration. (**A**) Flow cytometric analysis showing ASGPR surface expression on LT-EVs before and after immunomagnetic sorting. (**B**) Size distribution of LT-EVs analyzed by NTA. (**C**) Quantification of particle number of LT-EVs by NTA and protein amount of LT-EVs determined by the BCA assay. Mean ± SD. $n=3$ per group. *, $p<0.05$; ***, $p<0.001$; one-way ANOVA with Turkey's post-hoc tests. (**D**) Representative TEM image of LT-EVs from Sham and PHx livers. Bars = 250 nm. (**E**) Size distribution of sorted Hep-EVs analyzed by NTA. (**F**) Quantification of particle number of sorted Hep-EVs by NTA and protein amount determined by the BCA assay. Mean ± SD. $n=3$ per group. ***, $p<0.001$; ****, $p<0.0001$; one-way ANOVA with Turkey's post-hoc tests. (**G**) Venn diagram of proteome of PHx and Sham Hep-EVs. (**H**) Volcano plot of proteome of PHx and Sham Hep-EVs. (**I**) GO terms in the Cellular Component category of DEPs enriched in PHx over Sham Hep-EVs. (**J**) Western blot analysis of protein marker expression of LT-EVs and Hep-EVs. (**K**) Top-ranked DEPs of interest in Hep-EVs and Western blot validation of expression

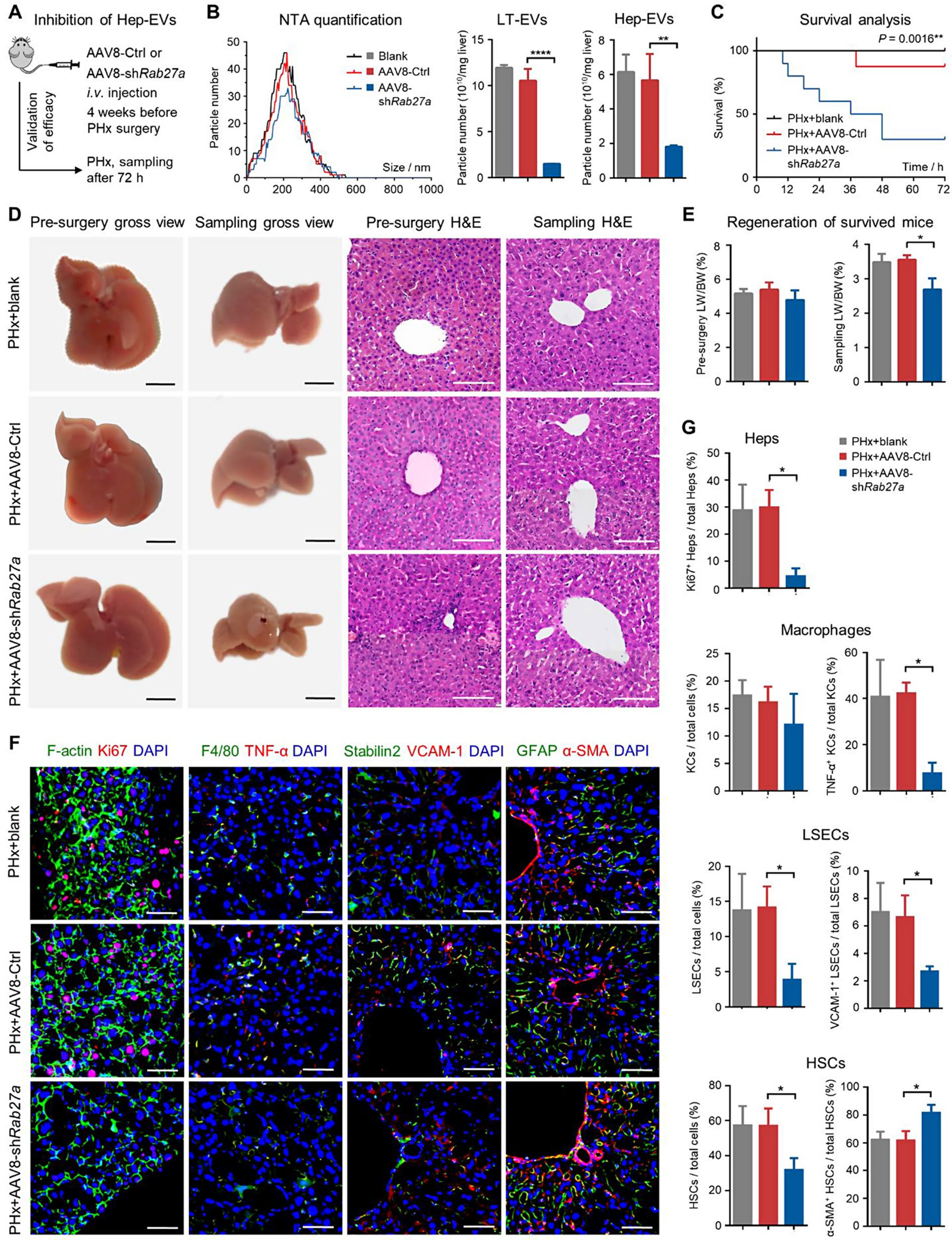

Fig. 4 (See legend on next page.)

(See figure on previous page.)

Fig. 4 Hep-EV release is indispensable for orchestrating liver regeneration. (**A**) Schematic diagram of the study design using AAV8-shRNA to inhibit hepatocyte *Rab27a via i.v.* injection at 4 weeks prior to PHx. (**B**) Quantification of particle number of LT-EVs and Hep-EVs determined by NTA. Hep-EVs were immunomagetically sorted from LT-EVs. Mean ± SD. $n = 3$ per group. **, $p < 0.01$; ****, $p < 0.0001$; one-way ANOVA with Turkey's post-hoc tests. (**C**) Kaplan-Meier survival analysis of mice. $n = 8$ per group. Log-rank test was used. (**D**) The gross view images and H&E staining of liver tissues. Bars = 500 mm (gross view) and 100 mm (H&E). (**E**) Quantification of liver weight over body weight ratio. Mean ± SD. $n = 3$ per group. *, $p < 0.05$; one-way ANOVA with Turkey's post-hoc tests. (**F**) IF staining of hepatocyte proliferation, macrophage inflammation, LSEC and HSC activation in the liver. Bars = 50 μm. (**G**) Quantification of percentages of proliferative hepatocytes, total and inflammatory macrophages, total and activated LSECs and HSCs in the liver. Mean ± SD. $n = 3$ per group. *, $p < 0.05$; one-way ANOVA with Turkey's post-hoc tests

Collectively, these findings indicate that hepatocytes significantly enhance EV release during liver regeneration.

We then analyzed the protein cargo profiles of Hep-EVs from Sham and PHx livers by performing liquid chromatography with tandem mass spectrometry (LC-MS/MS). A total of over 3,000 proteins were identified (Table S2). The Venn diagram indicated the presence of 3,357 shared proteins between Sham and PHx Hep-EVs, with 56 and 129 unique proteins identified in each group, respectively (Fig. 3G). Among the shared proteins, 387 were identified as differentially expressed proteins (DEPs; fold change > 1.5 and p-value < 0.05), with 193 DEPs upregulated and 184 downregulated in PHx Hep-EVs (Fig. 3H). This analysis highlighted clear separation and distinct protein signatures between Sham and PHx Hep-EVs (Figure S4A). GO enrichment analysis of DEPs in the Cellular Component (GO-CC) category revealed that annotations related to the proliferative process, such as "replication fork", "chromosomal, telomeric region", and "cytoplasmic microtubule", were particularly regulated terms in Hep-EVs during liver regeneration (Fig. 3I). Moreover, the functionality of DEPs was notably associated with "DNA replication" and "cell cycle" in the KEGG enrichment analysis, as well as several mitosis-related terms in the Biological Process (GO-BP) and Molecular Function (GO-MF) categories of GO databases (Figure S4B-D).

The above findings identified liver regeneration-associated cargo profiles of Hep-EVs, centered on proliferative regulation. To validate these data, we selected several top DEPs of interest for Western blot analysis (Fig. 3J). Not surprisingly, both LT-EVs and Hep-EVs from Sham and PHx mice expressed representative EV markers such as the tetraspanin surface molecule CD63, the lipid raft protein Flotillin-1, and the endosomal sorting complex required for transport (ESCRT)-associated protein, tumor suppressor gene 101 (TSG101) (Fig. 3K). Meanwhile, the Golgi component protein Golgin84, a negative EV marker, was not detected in either LT-EVs or Hep-EVs (Fig. 3K). Interestingly, PHx-derived Hep-EVs were confirmed to highly express the matrix protein Proteoglycan 4 (Prg4) and the Non-SMC condensin II complex subunit G2 (Ncapg2), which mediates the microtubule-attachment process to accelerate mitosis [24], despite not being enriched with the epigenetic enzyme DNA methyltransferase 1 (Dnmt1) and the DNA helicase Minichromosome maintenance complex component 3 (Mcm3) [25] (Fig. 3K). Notably, Cdk1, a critical kinase for promoting the G2/M and G1/S transitions, was especially enriched in both LT-EVs and Hep-EVs during liver regeneration (Fig. 3K). Taken together, these findings emphasize that Hep-EVs demonstrate enhanced release with proliferative information during liver regeneration.

Hep-EV release is indispensable for orchestrating liver regeneration

The aforementioned findings led us to explore whether Hep-EVs are functionally essential for liver regeneration. To investigate this, we constructed and intravenously (*i.v.*) administered the pAAV-ApoE/hAATp-*Rab27a*-shRNA to specifically inhibit the release of EVs by hepatocytes in vivo at 4 weeks before PHx (Fig. 4A). As anticipated, compared to the blank group and mice injected with the control vector, AAV8-mediated sh*Rab27a* delivery successfully reduced the quantity of LT-EVs and Hep-EVs (Fig. 4B). Crucially, targeted inhibition of Hep-EV release substantially reduced the survival rate of mice after PHx, with only 25% survival at 72 h, indicating diminished liver regeneration (Fig. 4C). Furthermore, gross analysis of livers from even the surviving mice at 72 h, along with histological examinations and quantification of liver weight over body weight ratio (LW/BW), confirmed delayed regeneration without tissue alterations following AAV8-mediated *Rab27a* knockdown (Fig. 4D and E). Indeed, IF staining also revealed that pAAV-ApoE/hAATp-*Rab27a*-shRNA delivery prevented hepatocytes from proliferating post-PHx challenge, underscoring the functional significance of Hep-EVs for liver parenchymal recovery (Fig. 4F and G). Additionally, AAV8-mediated *Rab27a* inhibition resulted in reduced inflammation in liver macrophages, decreased numbers of normal and activated LSECs, as well as reduced quiescent but increased activated HSCs, highlighting the essential role of Hep-EVs in coordinating immune, endothelial, and mesenchymal responses during liver regeneration (Fig. 4F and G). Collectively, these findings highlight that Hep-EV release is indispensable for orchestrating liver regeneration.

Hep-EVs from the regenerating liver reciprocally promote hepatocyte proliferation *via* Cdk1 activity

Next, we investigated the mechanism of Hep-EVs regulating liver regeneration. By integrating proteomic data of Hep-EVs and scRNA-seq data of their parental cells,

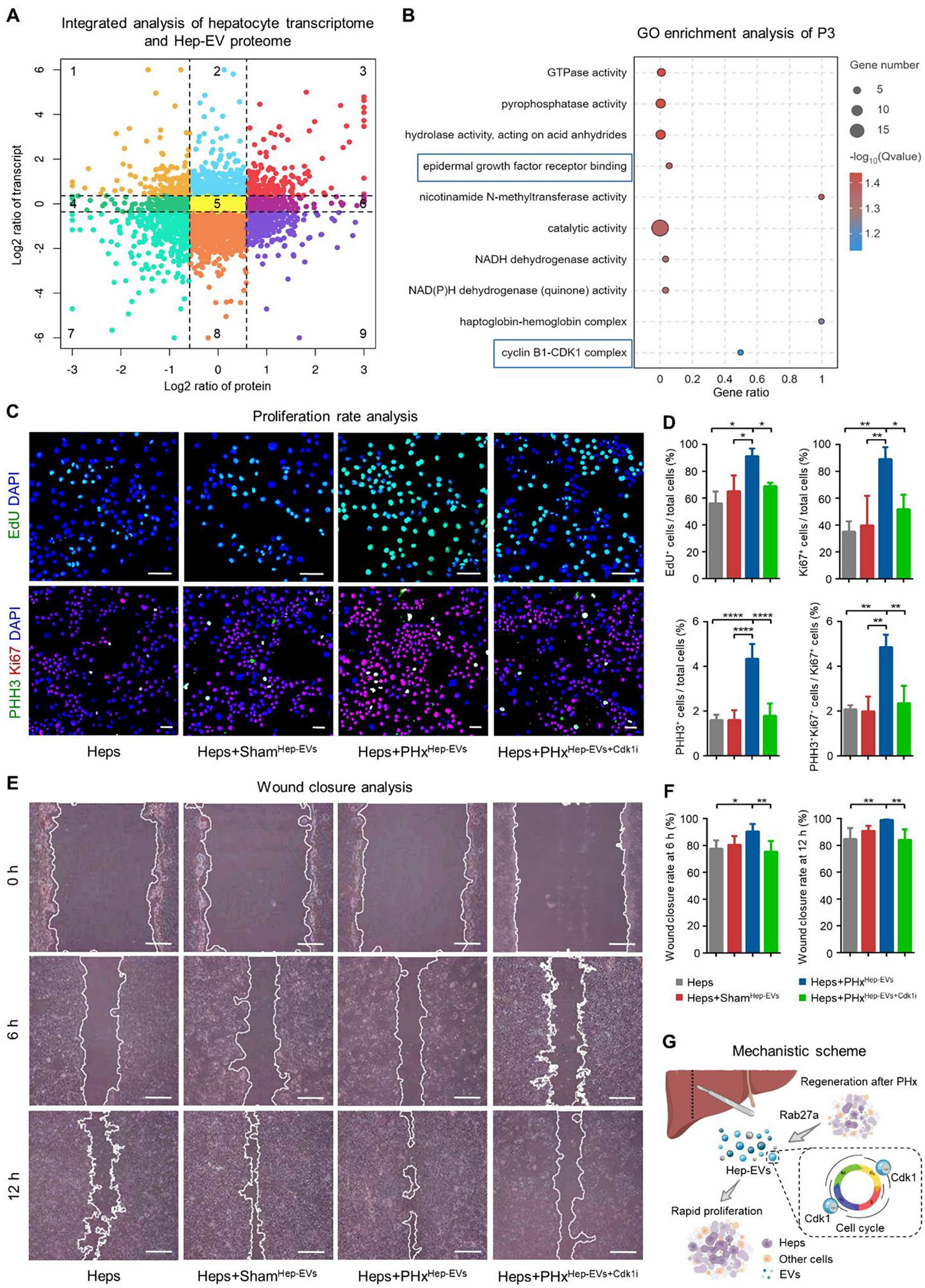

Fig. 5 (See legend on next page.)

(See figure on previous page.)

Fig. 5 Hep-EVs from the regenerating liver reciprocally promote proliferation of hepatocytes *via* Cdk1 activity. (**A**) Nine-quadrant diagram showing integrated analysis of hepatocyte transcriptome from scRNA-seq and Hep-EV proteome. (**B**) GO enrichment analysis of the P3 quadrant showing consistent upregulation of hepatocyte genes and Hep-EV proteins. (**C**) EdU assay and IF staining of PHH3 with Ki67 for proliferative hepatocytes treated with Hep-EVs and the Cdk1 inhibitor RO-3306. Bars = 100 μm. (**D**) Quantification of percentages of EdU^+, $Ki67^+$, $PHH3^+$ hepatocytes and $PHH3^+Ki67^+$ hepatocytes among $Ki67^+$ hepatocytes. $n = 3$ per group. *, $p < 0.05$; **, $p < 0.01$; ***, $p < 0.001$; ****, $p < 0.0001$; one-way ANOVA with Turkey's post-hoc tests. (**E**) Representative images of wound closure assay of hepatocytes treated with Hep-EVs and the Cdk1 inhibitor RO-3306. Bars = 250 μm. (**F**) Quantification of wound closure rates of hepatocytes. $n = 3$ per group. *, $p < 0.05$; **, $p < 0.01$; one-way ANOVA with Turkey's post-hoc tests. (**G**) Schematic diagram showing the mechanistic findings of this study

we conducted a nine-quadrant analysis to distinguish between cellular and vesicular expression patterns during liver regeneration. The analysis highlighted a specific quadrant of interest, P3, where upregulation was observed in both datasets (Fig. 5A). GO enrichment analysis of this quadrant showed an association with terms related to cellular activity, notably "epidermal growth factor receptor binding" and "cyclin B1-CDK1 complex", suggesting proliferation-related functionality (Fig. 5B). Intriguingly, the data indicated that organelle-related proteins were uniquely upregulated in Hep-EVs, independent of the cellular transcriptome (Figure S5A), while metabolism-related terms were consistently downregulated in both hepatocytes and their EVs during liver regeneration (Figure S5B). These findings suggest that EVs diversify the information derived from hepatocytes and inherit potential proliferative regulation capabilities during liver regeneration.

We then investigated whether PHx-derived Hep-EVs were indeed capable of regulating cell proliferation for liver regenerative repair. Although many liver cell populations were affected by Hep-EV inhibition in vivo (Fig. 4F), we focused on hepatocytes as putative reciprocal targets of Hep-EVs, given the critical role they play in liver regeneration through effective proliferation control [1]. Considering the proliferative information carried by PHx-derived Hep-EVs, particularly the Cdk1 enrichment (Figs. 3K and 5B), we tested whether PHx-derived Hep-EVs regulated target cell mitosis mediated by Cdk1 activity. To this end, cultured hepatocytes were treated with Hep-EVs from Sham and PHx livers, with PHx-derived Hep-EVs preconditioned with or without a chemical inhibitor of Cdk1. As anticipated, 5-ethynyl-2'-deoxyuridine (EdU) labeling analysis and Ki67 IF staining demonstrated that PHx-derived Hep-EVs significantly promoted DNA synthesis in cultured hepatocytes, while Sham-derived Hep-EVs did not (Fig. 5C and D). IF staining of Ki67 with Phosphohistone H3 (PHH3), which marks cells in the late G2 and M phases [26], further revealed that PHx-derived Hep-EVs, but not their Sham counterparts, accelerated hepatocyte mitosis (Fig. 5C and D). The effects of PHx-derived Hep-EVs on hepatocyte proliferation were suppressed by Cdk1 inhibitor pretreatment, as shown by reduced percentages of EdU, Ki67, and PHH3 positive cells (Fig. 5C and D), highlighting the role of Cdk1 in facilitating both the G1/S and G2/M transitions [27]. The cellular wound closure assay confirmed the beneficial effects of PHx-derived Hep-EVs, rather than Sham-derived Hep-EVs, on the healing capability of hepatocytes, which were also dependent on Cdk1 activity (Fig. 5E and F). Collectively, these findings suggest a mechanism that Hep-EVs from the regenerating liver reciprocally stimulate rapid hepatocyte proliferation *via* Cdk1 activity-based promotion of cell cycle progression (Fig. 5G).

Replenishment of Hep-EVs from the regenerating liver rescues insufficient liver regeneration

Finally, we investigated whether Hep-EVs have translational potential to promote liver regeneration upon infusion. As a proof-of-concept experiment, we intravenously administered liver tissue-isolated Hep-EVs to replenish diminished in vivo Hep-EVs in recipient AAV8-treated *Rab27a*-knockdown mice (Fig. 6A). Hep-EVs were injected at 24 h before PHx, and biodistribution analysis demonstrated remarkable liver enrichment of Hep-EVs post-infusion (Fig. 6B). Importantly, survival analysis showed that Hep-EV replenishment significantly promoted liver regeneration after PHx, with mice injected with PHx-derived Hep-EVs exhibiting higher survival rates compared to those receiving Sham-derived EVs (Fig. 6C). Further gross and histological analysis of livers from surviving mice in each group confirmed that PHx-derived Hep-EVs significantly enhanced liver regeneration upon infusion (Fig. 6D and E). The effects of Hep-EVs on promoting hepatocyte proliferation after replenishment were also observed by IF staining, where the infusion of both Sham-derived and PHx-derived Hep-EVs increased the Ki67-positive hepatocyte percentages in vivo, particularly with PHx-derived Hep-EVs (Fig. 6D and E). Taken together, these results suggest that replenishment of Hep-EVs from the regenerating liver rescues insufficient liver regeneration.

Discussion

The liver is responsible for maintaining metabolism and detoxification in the body and is highly regenerative [1, 2]. The process of liver regeneration involves complex intercellular communication [3, 28]. However, the mechanisms underlying this elaborate functional interaction are not yet fully understood. EVs are biologically active paracrine messengers that play dynamic roles in various

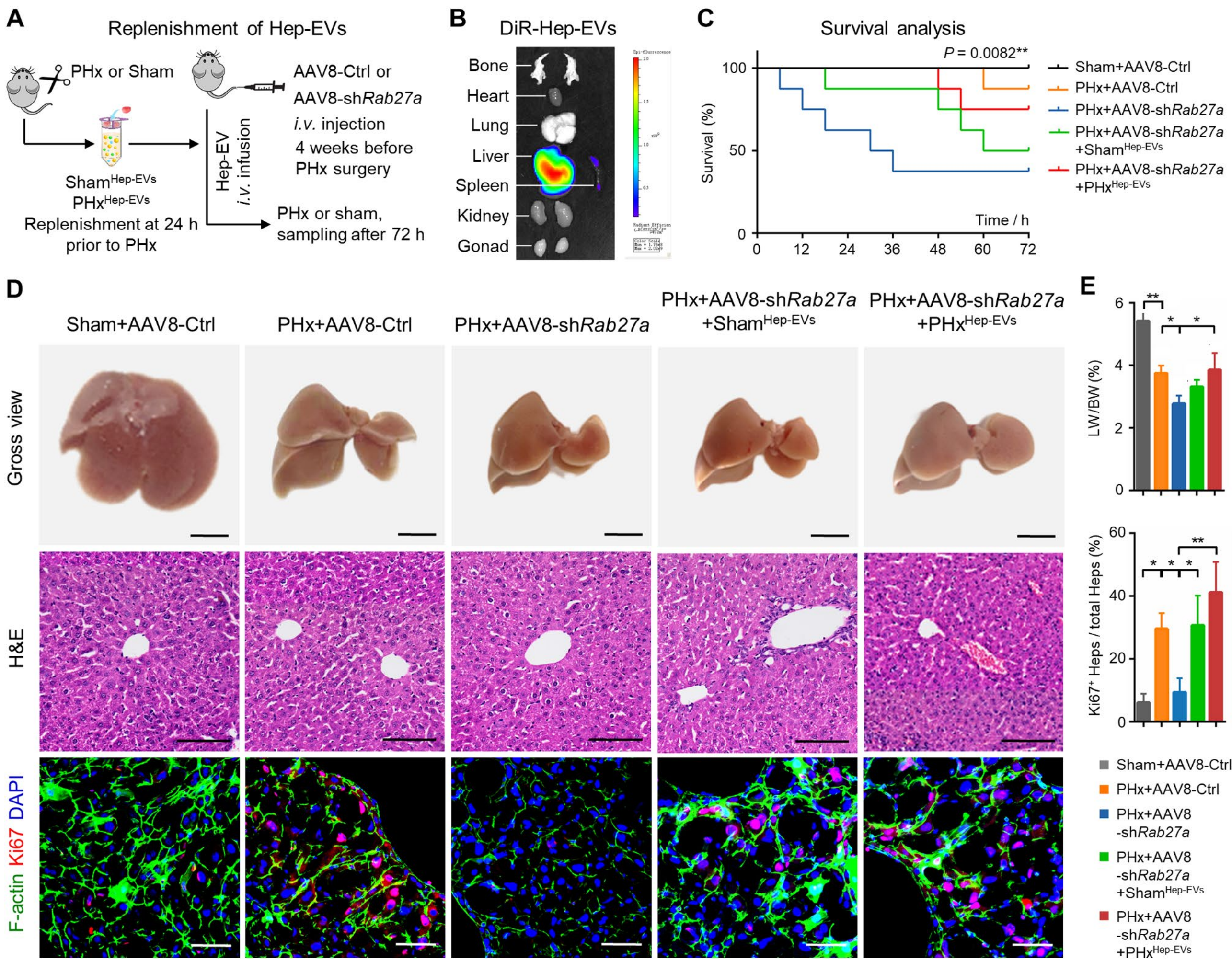

Fig. 6 Replenishment of Hep-EVs from the regenerating liver rescues insufficient liver regeneration. (**A**) Schematic diagram of the study design using Hep-EV infusion as a replenishment into AAV8-sh*Rab27a*-treated mice before liver regeneration analysis. (**B**) Biodistribution of DiR-labeled Hep-EVs at 24 h after infusion. (**C**) Kaplan-Meier survival analysis of mice. $n = 8$ per group. Log-rank test was used. (**D**) Gross view liver images, H&E staining of liver tissues, and IF staining of hepatocyte proliferation. Bars = 500 mm (gross view), 100 mm (H&E), and 50 µm (IF). (**E**) Quantification of liver weight over body weight ratio and percentages of proliferative hepatocytes. Mean ± SD. $n = 3$ per group. *, $p < 0.05$; **, $p < 0.01$; one-way ANOVA with Turkey's post-hoc tests

pathophysiological states [12, 13, 29–33]. In the present study, we mapped the transcriptomic landscape of liver regeneration at both bulk and single-cell levels, highlighting the crucial role of hepatocyte-centered intercellular communication mediated by EVs. Our investigation further revealed that liver regeneration promotes the release of LT-EVs, particularly Hep-EVs, which were confirmed both in situ and ex vivo to inherit regulated regenerative cues. Notably, Hep-EVs were demonstrated to promote hepatocyte proliferation in a reciprocal manner based on Cdk1 activity, which is essential in vivo for safeguarding liver regeneration both physiologically and upon therapeutic infusion. This study provides, for the first time, an integrated phenotypic and functional characterization of hepatocyte-specific tissue EVs in liver regeneration, offering insights into the biological and mechanistic aspects of the regenerating liver.

The liver possesses the remarkable ability to fully regenerate after undergoing partial resection [2]. Studies have documented that liver regeneration involves a combination of subsequent hepatocyte division, hypertrophy, and proliferation [8, 34]. Our sequencing data further suggested significant influences of liver regeneration on the metabolic processes of hepatocytes, which are largely suppressed in the regenerating liver. Indeed, the metabolic reprogramming after PHx represents an important event, and transcriptome sequencing combined with metabolomic analysis has indicated detailed metabolic changes during liver regeneration [35, 36]. Our findings, along with those of others, suggest that hepatocytes might sacrifice metabolic activity to safeguard regenerative expansion and are equipped with flexible metabolic machinery able to adapt dynamically to tissue regeneration [36]. It is also noteworthy that our data revealed the involvement of immune, endothelial, and stromal cell components in liver regeneration, which aligns with current understanding [3, 10, 37]. Additionally, communication between hepatocytes and various cell populations through EVs potentially contributes to liver regeneration. Future research is needed to examine in-depth the multimodal paracrine regulation mechanisms *via* Hep-EVs that safeguard liver regeneration.

Researchers worldwide have recently dedicated significant efforts to investigating EVs. These membranous nanoparticles are known to escape from the autophagy-lysosomal pathway and be released into the circulation and the extracellular space of tissues [38, 39]. Studies have particularly shown the potential of tissue EVs in promoting regeneration (Table S3). It has been reported that EVs from the brown adipose tissue (BAT) transfer miRNAs to protect cardiomyocytes against ischemia/reperfusion (IR) injury, while EVs from the white adipose tissue (WAT) benefit adipose tissue regeneration, suggesting context-dependent effects [40–42]. Cardiac tissue-derived EVs have also been shown to improve mitochondrial function to protect the heart against IR injury by delivering ATP5a1 [43]. This tissue-specific manner of EVs to promote tissue repair is further documented in the skin and the kidney [16]. With regard to LT-EVs, they have been employed to expedite the hepatic disease recovery process [17]. We have additionally proved the translational value of LT-EVs by their application in a bone defect model [44]. However, considering the heterogeneity of cell composition, the specific cellular origin of tissue EVs responsible for the regenerative action remains unknown. In this study, we established an immunomagnetic assay to specifically isolate Hep-EVs in the regenerating liver. Phenotypic assessments indicated that the isolation procedure did not significantly impact EV morphology and size distribution, suggesting that the properties of these tissue-derived EVs were largely maintained. With the advantages of potent specificity and efficiency [45–47], utilizing this approach in EV research will benefit biological and mechanistic investigations of endogenous tissue EVs, as well as diagnostic and therapeutic applications. Moreover, this approach can be applied to gain profound insights into crucial subsets of EVs, not only derived from specific cell sources but also possessing characteristic membrane proteins. Future examinations should elucidate the distinct functionalities of LT-EVs from diverse cell sources in liver health and disease.

The pivotal role EVs play in regulating liver health and disease has been suggested, but the function of endogenous LT-EVs remains not fully understood [48]. A recent study documented that interferon regulatory factor 1 (IRF1)-Rab27a-regulated EVs promote liver IR injury through surface oxidized phospholipids (OxPL) activation of neutrophils [49]. In our study, we also discovered that regenerative Hep-EVs are released under Rab27a control; however, the upstream molecular regulator of Rab27a following the PHx challenge remains to be investigated. Regarding the diversity of EVs contributing to liver regeneration, we previously uncovered that circulatory apoptotic vesicles (apoVs) safeguard liver regeneration by facilitating the organelle assembly of hepatocytes [22]. Other studies have revealed that PHx-induced apoVs stimulate neutrophils to secrete regenerative growth factors [50]. Here, we first reveal that Hep-EVs are functionally required to govern rapid hepatocyte proliferation in vivo and in vitro, and they show translational promise for promoting liver regeneration upon systemic infusion. It has been recently reported that EV cargoes are not randomly but specifically selected [51]. Notably, the Cdk1-based cell cycle control mechanism holds particular implications as a potential pharmacological target [27]. Cdk1, formerly known as Cell division cycle 2 (Cdc2), interacts with cyclin B1 to facilitate the transition from the G2 phase into mitosis, which has also the potential to promote G1/S progression by binding to cyclin E or cyclin D [52]. Cdk1 is the only CDK essential for the cell cycle in mammals [53]. In this study, using specific markers for DNA replication (Ki67 and EdU) and G2/M transition (PHH3), we demonstrated that Hep-EVs derived from the regenerating liver were capable of promoting both G1/S and G2/M transitions dependent on the Cdk1 activity, thus accelerating the cell cycle through an effective mechanism related to the donor tissue property. The effects of Hep-EV infusion on promoting liver regeneration are valuable for the translational use of tissue EVs in therapies.

In summary, our findings provide the first evidence that hepatocyte-specific tissue EVs are phenotypically involved in and functionally required for liver regeneration. Our study paves the way for in-depth biological and mechanistic research on regenerative Hep-EVs and sheds light on the role of physiological and endogenous tissue EV populations in organ regeneration and therapy.

Materials and methods

Animals

C57BL/6 male mice, 8 weeks of age, were utilized for this study. These mice were obtained from the Laboratory Animal Center of the Fourth Military Medical University. The mice were group-housed and maintained under specific pathogen-free conditions, with a standard 12-hour light/dark cycle and *ad libitum* access to food and water. All animal experiments were conducted in compliance with relevant laws and ethical regulations, adhering to the Guidelines of Intramural Animal Use and Care Committees of the Fourth Military Medical University, approved by the Ethics Committee of the Fourth Military Medical

University (Approval No. 2020-003), and in accordance with the ARRIVE guidelines.

PHx surgery

The PHx procedure was performed under sterile conditions [22]. Animals were anesthetized using isoflurane inhalation (R500IP, RWD Life Science, USA). For the 2/3 PHx, the median and left liver lobes were sequentially resected. The Sham operation involved a laparotomy. Sampling time points were established at 72 h throughout the study.

LT-EV collection and Hep-EV isolation

Tissue EVs were collected according to our previously published protocol [54]. Following 72 h post-Sham or PHx surgeries, mice were sacrificed, and liver tissues were gently dissociated into tiny pieces and then digested with Liberase TM enzyme (LIBTM-RO, Sigma-Aldrich, USA) for 30 min at 37 °C. This was followed by filtration through a 0.70-μm pore size filter. The filtrate was then centrifuged at 300 g for 10 min and at 2,000 g for 20 min at 4 °C to remove cells and tissue debris. The supernatant was further centrifuged at 16,800 g for 30 min at 4 °C to collect LT-EVs. For additional processing, LT-EVs were stained in the dark with ASGPR-PE antibody (sc-166633 PE, Santa Cruz Biotechnology, USA; diluted 1:100) at 4 °C for 4 h. Following staining, the LT-EVs were incubated with anti-PE magnetic microbeads (130-048-801, Miltenyi Biotec, USA) diluted 1:16 in MACS buffer (130-091-221, Miltenyi Biotec, USA) at 4 °C for 15 min. The mixture was then passed through an LD column (130-042-901, Miltenyi Biotec, USA) to capture $ASGPR^+$ LT-EVs (i.e., Hep-EVs). Captured Hep-EVs were transferred into fresh sterile tubes and subjected to two PBS washes. Finally, Hep-EVs were collected after centrifugation at 16,800 g for 30 min at 4 °C.

Hep-EV inhibition and replenishment in vivo

The liver-targeting AAV serotype 8 (AAV8), featuring a hepatocyte-specific promoter, human α1-antitrypsin promoter (hAATp), and an apolipoprotein E (ApoE) enhancer, was utilized to deliver shRNA specifically to knock down *Rab27a* in hepatocytes in vivo. Mice were injected through the tail vein with either an AAV vector carrying the *Rab27a* shRNA (pAAV-ApoE/hAATp-*Rab27a*-shRNA, Genechem, China) or a negative control vector (pAAV-ApoE/hAATp-null, Genechem, China) at a dose of 1×10^{11} v.g per 200 μl per mouse. These AAV injections occurred 4 weeks prior to the PHx and Hep-EV administration. For Hep-EV administration, Hep-EVs suspended in filtered PBS were injected *via* the caudal vein of the mouse at a dose of 5×10^{10} particles per 200 μl per mouse for 24 h, followed by the PHx surgery. For Hep-EV biodistribution analysis, Hep-EVs were stained by 5 μM DiR (Invitrogen, USA) before intravenous injection. Mice were euthanized after 24 h, and the tissues were examined using an in vivo imaging system (IVIS Lumina II, Caliper Life Science, USA).

Liver bulk RNA-seq analysis

The total RNA from the entire liver was extracted using the Trizol reagent kit (Invitrogen, USA) following the manufacturer's protocol. RNA quality was assessed using an Agilent 2100 Bioanalyzer (Agilent Technologies, USA) and verified through RNase free agarose gel electrophoresis. Subsequently, eukaryotic mRNA was enriched using Oligo (dT) beads. After total RNA was extracted, eukaryotic mRNA was enriched by Oligo (dT) beads. The enriched mRNA was then fragmented into short fragments using fragmentation buffer and reversely transcribed into cDNA using NEBNext Ultra RNA Library Prep Kit for Illumina (NEB #7530, New England Biolabs, USA). The purified double-stranded cDNA fragments were end repaired, addition of a base, and ligation to Illumina sequencing adapters. The ligation reaction was purified using the AMPure XP Beads (1.0X) and amplified through polymerase chain reaction (PCR). The resulting cDNA library was sequenced using Illumina Novaseq6000 by Gene Denovo Biotechnology Co. (Guangzhou, China). Genes/transcripts exhibiting false discovery rate (FDR) parameter below 0.05 and an absolute fold change ≥ 2 were considered differentially expressed genes/transcripts. Subsequent functional analysis was performed utilizing the GO and KEGG databases, or through GSEA enrichment analysis.

scRNA-seq microarray dataset

scRNA-seq microarray datasets were screened and downloaded from the Gene Expression Omnibus (GEO). The GSM4572241 and GSM4572243 series were obtained from the GEO database for analysis of DEGs. Further functional analysis was carried out based on the GO and KEGG databases.

Cell clustering

The cell-by-gene matrices for each sample were individually imported to Seurat version 3.1.1 for subsequent analysis. Seurat was utilized to conduct expression quality check, data normalization, t-distributed stochastic neighbor embedding (tSNE) plot analysis, cell clustering, cluster visualization, and cell type annotation.

Pseudotemporal trajectory analysis

The single-cell pseudotemporal trajectory [55, 56] was analyzed using matrices of cells and gene expressions by Monocle (Version 2.10.1). The space was reduced with two dimensions, and cells were ordered (sigma = 0.001, lambda = NULL, param.gamma = 10, tol = 0.001). The trajectory was visualized using a tree-like structure, including tips and branches.

Proteomic analysis

Protein lysates of Hep-EVs from Sham and PHx groups were prepared and subjected to liquid chromatography with tandem mass spectrometry (LC-MS/MS) analysis on an Orbitrap Exploris™ 480 mass spectrometer with a NanoSpray III ion source. The raw data were analyzed using the Proteome Discoverer system (v2.4.1.15). Proteins were identified by comparison with the Uniport database, with a false discovery rate set at 0.01 for both peptides and proteins. Quantification of proteins was performed using the default parameters in MaxQuant. Among the identified proteins, 516 proteins were DEPs (fold change > 1.5 and p-value < 0.05). These proteins were selected for further functional analysis based on GO and KEGG databases.

Cell culture and assays

The murine AML12 hepatocytes (ATCC CRL-2254) were cultured in Dulbecco's modified Eagle's medium with F-12 (DMEM F-12, Gibco, USA) at 37 °C with 5% CO_2. The medium was supplemented with 10% fetal bovine serum (FBS; HyClone, USA), 1% ITS liquid medium supplement (Sigma Aldrich, USA), 1% 100 µg/ml of penicillin and streptomycin (HyClone, USA), and 40 ng/ml of dexamethasone (Sigma-Aldrich, USA). Hep-EVs were used to treat AML12 cells for 48 h at a protein concentration of 10 µg/ml. The RO-3306 compound was dissolved in dimethyl sulfoxide (DMSO) (D8371, Solarbio, China) and added to Hep-EVs at a concentration of 5 µM for a duration of 24 h, then washed prior to Hep-EVs treatment.

For the wound closure assay, hepatocytes were seeded into 6-well plates at 5×10^5 cells/well. When the cells reached 90% confluence, sterile 200 µl pipette tips were used to create cell wounds on the plates. After washing with PBS, the medium was changed into culture medium without FBS and added with 10 µg/ml of Hep-EVs dissolved in PBS to specific wells for a duration of 48 h. Cells were photographed at 0 h, 6 h, and 12 h with an inverted microscope (Leica, Germany). Quantification of the wound area was performed using the ImageJ software (NIH, USA). For the EdU labeling assay, hepatocytes were seeded into 6-well plates at 5×10^5 cells/well. DNA synthesis was examined by 2-hour EdU labeling using a commercial kFluor488 Click-iT EdU kit (KGA331, KeyGEN, China). Quantification of the positively labeled cell percentages was performed using the ImageJ software (NIH, USA).

Integrated analysis of associations between genes and proteins

The genes/proteins and DEGs/DEPs detected in the scRNA-seq and proteomic analyses were enumerated. Subsequently, correlation analysis was conducted by R (version 3.5.1). A nine-quadrant map was generated based on the alternations in gene expression within the hepatocyte transcriptome and the Hep-EV proteome. Quantitative and enrichment analysis of genes in each quadrant was carried out.

TEM analysis

TEM was utilized to confirm the presence of EVs in the livers. Post-perfusion liver from the PHx and Sham mice were cut into pieces of approximately 1 mm × 1 mm × 1 mm, rapidly fixed in 3% glutaraldehyde, and post-fixed in a 1% OsO_4 solution at 4 °C. Following fixation, the samples were dehydrated with gradient acetone and embedded in araldite (EM TP, Leica, Germany). The sliced sections, prepared using an ultramicrotome (EM UC7, Leica, Germany), were stained with uranyl acetate and lead citrate and then examined with 120 KV TEM (JEM-1400FLASH, JEOL, Japan).

The morphology of LT-EVs was also characterized using TEM. A total of 4 µl of the EV solution, with a protein concentration of 1 mg/ml, was deposited onto a carbon-coated 400-square mesh copper grid. Ten minutes after the sample was deposited, the grid was rinsed with 10 drops of deionized water. Subsequently, a drop of 1% phosphotungstic acid (12501-23-4, RHAWN, China) was added to the grid to conduct the negative staining. The grid was then naturally dried and visualized using the 120 KV FEI TEM (TECNAI Spirit, FEI, USA). TEM-EDS was conducted using a field emission TEM (JEOL, Japan).

NTA experiments

The concentration and size distribution of LT-EVs and sorted Hep-EVs were analyzed by the Nanosight NS300 system (Malvern Panalytical, UK). Data were analyzed by Nanosight NTA 2.3 Analytical Software with the detection threshold optimized for each sample and screen gain at 10 to track as many particles as possible while maintaining minimal background interference. Additionally, a blank 0.2 µm-filtered PBS was run as a negative control for comparative analysis.

Western blot analysis

LT-EV and Hep-EV proteins were extracted using the RIPA lysis buffer (P0013B, Beyotime, China). The protein concentration of each sample was determined using the BCA protein assay kit (PA115, TIANGEN, China). Subsequently, all samples were prepared at a final concentration of 1 µg/µl in a loading buffer (CW0027S, CwBio, China). For protein separation based on molecular weight, 20 μg of protein samples were loaded into a 4–20% SDS-polyacrylamide gel (LK206, Epizyme, USA) within the Bio-Rad Electrophoresis System. The proteins within the gel were then transferred to polyvinylidene difluoride (PVDF) membranes. Following blocking in 5% bovine serum albumin (BSA) solution (218072801, MP Biomedical, USA), the membranes were subjected to overnight incubation at 4 °C with primary antibodies including CD63 (SC5275, Santa Cruz Biotechnology, USA), TSG101 (ab125011, Abcam, UK), Flotilin-1 (18634 S, Cell Signaling Technology, USA), Golgin84 (NBP1-83352, Novus Biologicals, USA), Dnmt1 (5032T, Cell Signaling Technology, USA), Ncapg2 (24563-1-AP, Proteintech, China), Mcm3 (A1060, Abclone, China), Prg4 (PA3-118, Invitrogen, USA), or Cdk1 (ab18, Abcam, UK). Subsequent to this, the PVDF membranes were subjected to incubation with corresponding secondary antibodies (Jackson ImmunoResearch, USA) for 1 h at room temperature. Finally, the PVDF membranes were imaged using Western chemiluminescent horseradish peroxidase (HRP) substrate (Millipore, USA) with an imaging system (Tanon 4600, Shanghai, China).

Flow cytometric analysis

The collected LT-EVs were subjected to staining for ASGPR (sc-166633, Santa Cruz Biotechnology, USA), F4/80 (ab6640, Abcam, UK), CD11b (101201, BioLegend, USA), CD31 (102407, BioLegend, USA), GFAP (38014, SAB, China), CK19 (60187-1, Proteintech, China), CD3 (100235, BioLegend, USA), or CD19 (152420, BioLegend, USA) using primary antibodies and their respective isotype control, including PE Mouse IgG2b,κ Isotype Ctrl Antibody (400312, BioLegend, USA), APC Mouse IgG2b,κ Isotype Ctrl Antibody (981906, BioLegend, USA), or Biotin Mouse IgG2b,κ Isotype Ctrl Antibody (401203, BioLegend, USA), at a concentration of 1:100 for 1 h at 4°C. Subsequently, fluorescence-conjugated secondary antibodies were applied. Following PBS washing, the percentages of positively stained LT-EVs were determined using a flow cytometer (NovoCyte; ACEA Biosciences, USA) and analyzed using NovoExpress software.

IF staining

Fresh liver tissue samples were fixed in 4% paraformaldehyde (PFA) (Biosharp, China) at 4 °C for 4 h, washed with PBS, and dehydrated with 30% sucrose for 24 h. After dehydration, the samples were embedded in an optimal cutting temperature (OCT) compound (Leica, Germany), and 10 μm cryosections were prepared using a Cryostat (CM1950, Leica, Germany). The air-dried cryosections were permeabilized by 0.3% Triton X-100 (Sigma-Aldrich, USA) for 20 min at room temperature, following by blocking in goat serum (Boster, China) for 30 min at room temperature. The cryosections were then incubated with the following primary antibodies overnight at a concentration of 1:100 at 4 °C: rabbit anti-mouse Ki67 primary antibody (ab15580, Abcam, UK), rat anti-mouse F4/80 primary antibody (ab6640, Abcam, UK), mouse anti-mouse TNF-α primary antibody (ab1793, Abcam, UK), rabbit anti-mouse VCAM-1 primary antibody (A19131, Abclonal, China), rat anti-mouse Stabilin2 primary antibody (D17-3, Medical & Biological Laboratories, Japan), mouse anti-mouse GFAP primary antibody (38014, SAB, China), rabbit anti-mouse α-SMA primary antibody (ab124964, Abcam, UK) overnight at a concentration of 1:100 at 4 °C. After washing with PBS, sections were then stained with the following fluorescence-conjugated secondary antibodies at a concentration of 1:200 at 4 °C for 1 h at room temperature: Alexa Fluor 594-conjugated donkey anti-rabbit secondary antibody (R37119, Invitrogen, USA), Alexa Fluor 488-conjugated goat anti-mouse secondary antibody (A-11001, Invitrogen, USA), Alexa Fluor 594-conjugated goat anti-mouse secondary antibody (A-11005, Invitrogen, USA), Alexa Fluor 488-conjugated chicken anti-rat secondary antibody (A-21470, Invitrogen, USA). Additionally, for F-actin staining of hepatocyte borders, after washing with PBS, sections were probed with phalloidin conjugated to Alexa Fluor 488 (R37110, Invitrogen, USA) according to the manufacturer's instructions, and counterstained with 4,6-diamidino-2-phenylindole (DAPI) (ab104139, Abcam, UK). The liver tissues were imaged by CLSM (A1plus, Nikon, Japan) and analyzed using the ImageJ software (NIH, USA).

Cultured AML12 hepatocytes were washed with PBS for three times, and fixed with 4% PFA for 30 min at room temperature, followed by washing with PBS and blocking in goat serum for 30 min at room temperature. Cells were incubated with the following primary antibodies overnight at a concentration of 1:100 at 4 °C: rabbit anti-mouse Ki67 primary antibody (ab15580, Abcam, UK), rat anti-mouse PHH3 primary antibody (66863-1-lg, Proteintech, China. After washing with PBS, the cells were stained with the following fluorescence-conjugated secondary antibodies at room temperature for 1.5 h: Alexa Fluor 594-conjugated donkey anti-rabbit secondary antibody (R37119, Invitrogen, USA), Alexa Fluor 488-conjugated goat anti-mouse secondary antibody (A-11001, Invitrogen, USA. Subsequently, the cells were washed with PBS and their nuclei were counterstained with DAPI (ab104139, Abcam, UK). Fluorescence imaging was carried out by CLSM (A1plus, Nikon, Japan) and analyzed using the ImageJ software (NIH, USA).

Histological staining

Fresh liver tissue samples were fixed in 4% PFA for 24 h and then washed with running water to remove excess PFA. Then, the samples underwent dehydration through graded ethanol and were embedded in paraffin. They were then sectioned at 5 μm per slice. H&E staining was performed with a commercial staining kit (Baso Technology, China). Images of the stained samples were captured using the SLIDEVIEW VS200 (Olympus, Japan).

Statistical analysis

All data were expressed as mean ± standard deviation (SD). Statistical comparisons between data sets were conducted with an analysis of normality and variance, followed by a two-tailed unpaired Student's *t* test for two-group comparisons and one-way ANOVA with Turkey's post-hoc tests for multiple group comparisons using the GraphPad Prism 9.0.0 software. Survival rates were analyzed using the Log-rank test. A difference was considered statistically significant when $p < 0.05$.

Supplementary Information

The online version contains supplementary material available at https://doi.org/10.1186/s12951-024-02790-0.

Supplementary Material 1

Supplementary Material 2

Supplementary Material 3

Supplementary Material 4

Acknowledgements

This work was supported by grants from the National Natural Science Foundation of China (82371020, 82301028, 81930025 and 82170988), the Young Science and Technology Rising Star Project of Shaanxi Province (2023KJXX-027), and the China Postdoctoral Science Foundation (BX20230485). We are grateful for the assistance of the National Experimental Teaching Demonstration Center for Basic Medicine (AMFU). We thank PTM Biolabs Co., Ltd (Hangzhou, China) for help in analyzing the proteomic data. We thank Mr. Tao Liu (Gene Denovo Biotechnology Co, Ltd, 790 Guangzhou, China) for his assistance in analyzing the single-cell sequencing data.

Author contributions

S.Q.Y. and Y.C. contributed equally to the design and conduction of the study and drafted the manuscript. Z.K.Z. and X.Y.L. analyzed and interpreted data. X.H.Z. contributed to the transcriptomic and scRNA-seq experiments. K.S. performed partial hepatectomy. J.Y.Q. contributed to NTA and WB experiments. S.J.X. contributed to H&E and IF experiments. Y.Y.L. contributed to TEM and flow cytometry analysis. K.Z. contributed to the proteomic experiment. F.J. contributed to the discussion and interpretation of data. C.X.Z., Y.J. and B.D.S. conceived the project, designed and supervised the experiments. All authors revised the manuscript and approved the final version.

Data availability

Sequence data that support the findings of this study are provided as supplementary table files. All other data included in this study are available upon reasonable request of corresponding authors.

Declarations

Ethical approval

This study was approved by the Ethics Committee of the Fourth Military Medical University (Approval No. 2020-003).

Competing interests

The authors declare no competing interests.

Received: 19 June 2024 / Accepted: 20 August 2024
Published online: 30 August 2024

References

1. Michalopoulos GK, Bhushan B. Liver regeneration: biological and pathological mechanisms and implications. Nat Rev Gastroenterol Hepatol. 2021;18:40–55.
2. Michalopoulos GK. Liver regeneration after partial hepatectomy: critical analysis of mechanistic dilemmas. Am J Pathol. 2010;176:2–13.
3. Campana L, Esser H, Huch M, Forbes S. Liver regeneration and inflammation: from fundamental science to clinical applications. Nat Rev Mol Cell Biol. 2021;22:608–624.
4. Ait Ahmed Y, Fu Y, Rodrigues RM, He Y, Guan Y, Guillot A, et al. Kupffer cell restoration after partial hepatectomy is mainly driven by local cell proliferation in IL-6-dependent autocrine and paracrine ma nners. Cell Mol Immunol. 2021;18:2165–2176.
5. Shimizu H, Miyazaki M, Wakabayashi Y, Mitsuhashi N, Kato A, Ito H, et al. Vascular endothelial growth factor secreted by replicating hepatocytes induces sinusoidal endothelial cell proliferation during regeneration after partial hepatectomy in rats. J Hepatol. 2001;34:683–689.
6. Xiao T, Meng W, Jin Z, Wang J, Deng J, Wen J, et al. Mir-182-5p promotes hepatocyte-stellate cell crosstalk to facilitate liver regeneration. Commun Biology. 2022;5:771.
7. Song J, Ma J, Liu X, Huang Z, Li L, Li L, et al. The MRN complex maintains the biliary-derived hepatocytes in liver regeneration through ATR-Chk1 pathway. NPJ Regenerative Med. 2023;8:20.
8. Yanger K, Knigin D, Zong Y, Maggs L, Gu G, Akiyama H, et al. Adult hepatocytes are generated by self-duplication rather than stem cell differentiation. Cell Stem Cell. 2014;15:340–349.
9. Mei Y, Thevananther S. Endothelial nitric oxide synthase is a key mediator of hepatocyte proliferation in response to partial hepatectomy in mice. Hepatology. 2011;54:1777–1789.
10. Forbes SJ, Newsome PN. Liver regeneration - mechanisms and models to clinical application. Nat Rev Gastroenterol Hepatol. 2016;13:473–485.
11. Stravitz RT, Lee WM. Acute liver failure. Lancet. 2019;394:869–881.
12. Mager SELA, Breakefield I, Wood XO. Extracellular vesicles: biology and emerging therapeutic opportunities. Nat Rev Drug Discovery. 2013;12:347–357.
13. Yanez-Mo M, Siljander PR, Andreu Z, Zavec AB, Borras FE, Buzas EI, et al. Biological properties of extracellular vesicles and their physiological functions. J Extracell Vesicles. 2015;4:27066.
14. Qin B, Hu XM, Su ZH, Zeng XB, Ma HY, Xiong K. Tissue-derived extracellular vesicles: Research progress from isolation to application. Pathol Res Pract. 2021;226:153604.
15. Li SR, Man QW, Gao X, Lin H, Wang J, Su FC, et al. Tissue-derived extracellular vesicles in cancers and non-cancer diseases: Present and future. J Extracell Vesicles. 2021;10:e12175.
16. Lou P, Liu S, Wang Y, Lv K, Zhou X, Li L, et al. Neonatal-tissue-derived extracellular vesicle therapy (NEXT): a potent strategy for Precision Regenerative Medicine. Adv Mater. 2023;35:e2300602.
17. Lee J, Kim SR, Lee C, Jun YI, Bae S, Yoon YJ, et al. Extracellular vesicles from in vivo liver tissue accelerate recovery of liver necrosis induced by carbon tetrachloride. J Extracell Vesicles. 2021;10:e12133.
18. Verweij FJ, Balaj L, Boulanger CM, Carter DRF, Compeer EB, D'Angelo G, et al. The power of imaging to understand extracellular vesicle biology in vivo. Nat Methods. 2021;18:1013–1026.
19. Crescitelli R, Lasser C, Lotvall J. Isolation and characterization of extracellular vesicle subpopulations from tissues. Nat Protoc. 2021;16:1548–1580.
20. Vella LJ, Scicluna BJ, Cheng L, Bawden EG, Masters CL, Ang CS, et al. A rigorous method to enrich for exosomes from brain tissue. J Extracell Vesicles. 2017;6:1348885.
21. Nojima H, Freeman CM, Schuster RM, Japtok L, Kleuser B, Edwards MJ, et al. Hepatocyte exosomes mediate liver repair and regeneration via sphingosine-1-phosphate. J Hepatol. 2016;64:60–68.
22. Sui B, Wang R, Chen C, Kou X, Wu D, Fu Y, et al. Apoptotic vesicular metabolism contributes to Organelle Assembly and safeguards Liver Homeostasis and Regeneration. Gastroenterology; 2024.
23. Welsh JA, Goberdhan DCI, O'Driscoll L, Buzas EI, Blenkiron C, Bussolati B, et al. Minimal information for studies of extracellular vesicles (MISEV2023): from basic to advanced approaches. J Extracell Vesicles. 2024;13:e12404.

24. Wang Q, Li Z, Zhou S, Li Z, Huang X, He Y, et al. NCAPG2 could be an immunological and prognostic biomarker: from pan-cancer analysis to pancreatic cancer validation. Front Immunol. 2023;14:1097403.
25. Alvarez S, Diaz M, Flach J, Rodriguez-Acebes S, Lopez-Contreras AJ, Martinez D, et al. Replication stress caused by low MCM expression limits fetal erythropoiesis and hematopoietic stem cell functionality. Nat Commun. 2015;6:8548.
26. Elmaci I, Altinoz MA, Sari R, Bolukbasi FH. Phosphorylated histone H3 (PHH3) as a novel cell proliferation marker and prognosticator for meningeal tumors: a short review. Appl Immunohistochem Mol Morphol. 2018;26:627–631.
27. Lukasik P, Zaluski M, Gutowska I. Cyclin-dependent kinases (CDK) and their role in diseases Development-Review. Int J Mol Sci 2021;22.
28. Wang R, Peng X, Yuan Y, Shi B, Liu Y, Ni H, et al. Dynamic immune recovery process after liver transplantation revealed by single-cell multi-omics analysis. Innov (Camb). 2024;5:100599.
29. Jiang J, Mei J, Ma Y, Jiang S, Zhang J, Yi S, et al. Tumor hijacks macrophages and microbiota through extracellular vesicles. Explor (Beijing). 2022;2:20210144.
30. Kwaku GN, Ward RA, Vyas JM, Harding HB. Host innate immune systems gather intel on invading microbes via pathogen-derived extracellular vesicles. Extracell Vesicle 2024;3.
31. Park HJ, Kelly JM, Hoffman JR, Takaesu F, Schwartzman W, Ulziibayar A et al. Computational analysis of serum-derived extracellular vesicle miRNAs in juvenile sheep model of single stage Fontan procedure. Extracell Vesicle 2022;1.
32. Hook V, Podvin S, Mosier C, Boyarko B, Seyffert L, Stringer H, et al. Emerging evidence for dysregulated proteome cargoes of tau-propagating extracellular vesicles driven by familial mutations of tau and presenilin. Extracell Vesicles Circ Nucl Acids. 2023;4:588–598.
33. Aafreen S, Feng J, Wang W, Liu G. Theranostic extracellular vesicles: a concise review of current imaging technologies and labeling strategies. Extracell Vesicles Circ Nucl Acids. 2023;4:107–132.
34. Miyaoka Y, Ebato K, Kato H, Arakawa S, Shimizu S, Miyajima A. Hypertrophy and unconventional cell division of hepatocytes underlie liver regeneration. Curr Biol. 2012;22:1166–1175.
35. Li Z, Peng B, Chen S, Li J, Hu K, Liao L, et al. Transcriptome sequencing and metabolome analysis reveal the metabolic reprogramming of partial hepatectomy and extended hepatectomy. BMC Genomics. 2023;24:532.
36. Caldez MJ, Van Hul N, Koh HWL, Teo XQ, Fan JJ, Tan PY, et al. Metabolic remodeling during liver regeneration. Dev Cell. 2018;47:425–38. e425.
37. Matchett KP, Wilson-Kanamori JR, Portman JR, Kapourani CA, Fercoq F, May S, et al. Multimodal decoding of human liver regeneration. Nature. 2024;630:158–165.
38. Cao Y, Ying SQ, Qiu XY, Guo J, Chen C, Li SJ, et al. Proteomic analysis identifies Stomatin as a biological marker for psychological stress. Neurobiol Stress. 2023;22:100513.
39. Perrin P, Janssen L, Janssen H, van den Broek B, Voortman LM, van Elsland D, et al. Retrofusion of intralumenal MVB membranes parallels viral infection and coexists with exosome release. Curr Biol. 2021;31:3884–93. e3884.
40. Zhao H, Chen X, Hu G, Li C, Guo L, Zhang L, et al. Small extracellular vesicles from Brown Adipose tissue mediate Exercise Cardioprotection. Circ Res. 2022;130:1490–1506.
41. Dong J, Wu B, Tian W. Adipose tissue-derived small extracellular vesicles modulate macrophages to improve the homing of adipocyte precursors and endothelial cells in adipose tissue regeneration. Front Cell Dev Biol. 2022;10:1075233.
42. He C, Dai M, Zhou X, Long J, Tian W, Yu M. Comparison of two cell-free therapeutics derived from adipose tissue: small extracellular vesicles versus conditioned medium. Stem Cell Res Ther. 2022;13:86.
43. Liu X, Meng Q, Shi S, Geng X, Wang E, Li Y, et al. Cardiac-derived extracellular vesicles improve mitochondrial function to protect the heart against ischemia/reperfusion injury by delivering ATP5a1. J Nanobiotechnol. 2024;22:385.
44. Li CH, Lei X, Zheng CX, Jin Y, Sui BD, Ying SQ. Study on liver tissue derived-extracellular vesicles regulating the osteogenic differentiation ability of mesenchymal stem cells and promoting the healing of jaw bone defects. Zhonghua Kou Qiang Yi Xue Za Zhi. 2024;59:435–443.
45. Tang P, Thongrom B, Arora S, Haag R. Polyglycerol-based Biomedical Matrix for Immunomagnetic circulating Tumor Cell isolation and their expansion into Tumor spheroids for Drug Screening. Adv Healthc Mater. 2023;12:e2300842.
46. Shin HS, Park J, Lee SY, Yun HG, Kim B, Kim J et al. Integrative Magneto-Microfluidic Separation of Immune Cells Facilitates Clinical Functional Assays. Small. 2023:e2302809.
47. Huang Y, Arab T, Russell AE, Mallick ER, Nagaraj R, Gizzie E, et al. Toward a human brain extracellular vesicle atlas: characteristics of extracellular vesicles from different brain regions, including small RNA and protein profiles. Interdiscip Med. 2023;1:e20230016.
48. Balaphas A, Meyer J, Sadoul R, Morel P, Gonelle-Gispert C, Buhler LH. Extracellular vesicles: future diagnostic and therapeutic tools for liver disease and regeneration. Liver Int. 2019;39:1801–1817.
49. Yang MQ, Du Q, Goswami J, Varley PR, Chen B, Wang RH, et al. Interferon regulatory factor 1-Rab27a regulated extracellular vesicles promote liver ischemia/reperfusion injury. Hepatology. 2018;67:1056–1070.
50. Brandel V, Schimek V, Gober S, Hammond T, Brunnthaler L, Schrottmaier WC, et al. Hepatectomy-induced apoptotic extracellular vesicles stimulate neutrophils to secrete regenerative growth factors. J Hepatol. 2022;77:1619–1630.
51. Dixson AC, Dawson TR, Di Vizio D, Weaver AM. Context-specific regulation of extracellular vesicle biogenesis and cargo selection. Nat Rev Mol Cell Biol. 2023;24:454–476.
52. Malumbres M. Cyclin-dependent kinases. Genome Biol. 2014;15:122.
53. Santamaria D, Barriere C, Cerqueira A, Hunt S, Tardy C, Newton K, et al. Cdk1 is sufficient to drive the mammalian cell cycle. Nature. 2007;448:811–815.
54. Cao Y, Qiu JY, Chen D, Li CY, Xing SJ, Zheng CX et al. Isolation and analysis of Traceable and Functionalized Extracellular vesicles from the plasma and solid tissues. J Vis Exp 2022.
55. Su D, Jiao Z, Li S, Yue L, Li C, Deng M, et al. Spatiotemporal single-cell transcriptomic profiling reveals inflammatory cell states in a mouse model of diffuse alveolar damage. Explor (Beijing). 2023;3:20220171.
56. Akinlalu A, Flaten Z, Rasuleva K, Mia MS, Bauer A, Elamurugan S, et al. Integrated proteomic profiling identifies amino acids selectively cytotoxic to pancreatic cancer cells. Innov (Camb). 2024;5:100626.

Publisher's note